•机械工程•

**DOI:**10.12454/j.jsuese.202600009

本刊网刊

# 阵列气囊碰撞能量耗散与接触力抑制特性分析

钟　友[1,2],杨思昀[1,2],薛　淼[1,2],唐　雷[1,2],蒲　伟[1,2,3*],张　印[1,2*]

(1.四川大学 空天科学与工程学院,四川 成都 610207;2.空间先进机构与智能飞行器教育部重点实验室,四川 成都 610207;
3.四川大学 机械工程学院,四川 成都 610065)

**摘　要:**在轨服务与维护、空间碎片清理等任务中,航天器碰撞接触扰动的有效抑制是保障作业安全与精度的关键。传统电磁阻尼、弹簧阻尼等刚性缓冲结构凭借响应速度快、能量耗散效率高的优势,在航天工程中得到广泛应用,在碰撞能量耗散方面表现出良好性能。然而,受刚性材料本征特性限制,这类结构可适应的相对碰撞速度范围较窄,在高动态、变工况的空间碰撞场景中,存在接触力峰值突变、自适应调控能力不足的问题,难以兼顾宽工况下的力抑制与能量耗散要求。针对上述技术局限,本文提出一种基于阵列气囊的柔性缓冲结构,通过多气囊单元的协同变形与内部气体压缩效应,实现碰撞能量的自适应耗散与接触力的动态调控,建立了气囊单元及阵列的碰撞动力学模型,分析了初始动能、预充气压力等参数对能量耗散效率与力抑制特性的影响,揭示了多气囊协同工作机制下的能量和接触力传递规律。研究结果表明,该阵列气囊结构在初始动能为1.2 J以内的碰撞条件下,通过调节不同预充压力组合,将接触力峰值有效降低至1.1 N/cm$^2$,能量耗散率达95%以上,可为航天器柔性缓冲机构设计提供参考。

**关键词:**阵列气囊;动力学建模;接触力;能量耗散;在轨服务

**中图分类号:**V448.2;O313　　**文献标志码:**A　　**文章编号:**2096-3246(2026)06-0340-10

随着人类航天活动日益频繁,在轨航天器的规模与复杂度不断提升,其长期在轨运行期间面临的故障风险与寿命限制问题也愈加突出。在轨服务与维护系统可为故障航天器提供延寿、组件更换、移位等服务,实现对空间资产的持续维护和再利用,减缓轨道资源的紧张[1]。然而,当目标航天器因故障失效成为非合作目标(如失控翻滚、无专用对接接口)时,对其进行安全、可靠的捕获十分重要[2–3]。捕获过程中,服务航天器与目标航天器间难以避免地会发生接触碰撞,容易造成结构损伤或任务失败[4]。因此,如何实现碰撞能量的快速、可控耗散,有效抑制接触力,是发展空间目标安全操控技术的关键。

围绕非合作目标捕获,根据是否与目标发生接触,捕获方法可分为非接触式和接触式两大类[5]。其中,非接触式捕获以发射激光、离子束等方式产生作用力,推动目标到达期望位置或减缓其速度,适合无需在轨维护的空间碎片清理与减缓任务[6–7]。若目标被捕获后需要进一步精细作业,一般采用“卫星平台+刚性机械臂+末端工具”的接触式捕获方式。实践表明,基于机械臂的接触式捕获方法可实现任务平台与目标物体的稳固连接,便于执行在轨维修、维护等操作[8]。但由于机械臂及末端工具、被捕目标均为刚性结构和材料,捕获非合作目标时,必须避免机械臂与目标航天器发生激烈的接触碰撞。为了降低碰撞接触对捕获效果的负面影响,国内外学者在捕获机构设计、最优控制、精确建模等方面做了相关研究,取得了系列研究进展。

捕获机构设计方面,现有研究多以阻尼缓冲为优化方向,通过调节气压调控阻尼特性,进而缓冲碰撞冲击,实现目标的平稳捕获。例如,潘正伟[9]设计基于弹簧阻尼的四连杆捕获机构,孙冲等[10]提出依托材料固有阻尼的三爪捕获机构,尹航等[11]则研发集成磁流变阻尼器的柔性捕获机构,Zhang等[12]提出一种基于柔性气囊的指–掌协同抓手。

**收稿日期:**2026 – 01 – 06　　**修回日期:**2026 – 03 – 11　　**网络出版日期:**2026 – 03 – 25

**基金项目:**国家自然科学基金项目(52405030;52275206)

**作者简介:**钟　友(2000—),男,硕士生. 研究方向:柔性机器人设计与动力学分析. E-mail: scuzhongyou@foxmail.com

* **通信作者:**蒲　伟,教授,E-mail: pwei@scu.edu.cn;张　印,副研究员,E-mail: zyin@scu.edu.cn

接触碰撞能量调控的控制方法中，PID控制因原理简单、鲁棒性强而应用最广[13]。阻抗控制作为经典柔顺控制策略亦被广泛采用，Nenchev等[14]分析了捕获目标过程的碰撞冲击效应的影响因素和捕获后系统的控制；董楸煌等[15]在此基础上分析了空间机械臂捕获卫星的冲击效应。但现有研究对接触碰撞过程的分析局限于低碰撞速度，在高动态场景中面临适应性约束。

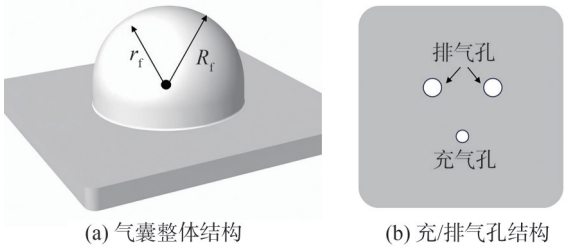
建立接触式捕获碰撞行为的理论模型，并掌握全过程动力学特性，是实现碰撞扰动精准调控的关键途径。为此，国内外学者对碰撞动力学建模方法进行了广泛研究，在多体接触碰撞动力学方面，普遍采用冲量动量法、连续碰撞力模型或基连续介质力学的有限元方法[16]，而在分析刚柔体接触过程计算接触力时，通常使用基于赫兹接触理论的改进型柔顺接触力模型[17–22]。

总的来看，现有非合作目标接触式捕获的研究和工程实现都在可靠捕获和避免激烈碰撞间权衡，本质上是要着力解决与目标发生的激烈碰撞扰动问题。为此，本文提出一种基于阵列气囊的柔性缓冲结构，通过多气囊协同变形与气体压缩，实现能量的自适应耗散与接触力动态调控，建立综合考虑气囊结构大变形、内部气体状态变化以及非线性接触的系统动力学模型。基于此模型，重点从接触力响应与动能耗散两个维度，分析在接触式捕获中关键设计参数对柔性阵列气囊缓冲性能的影响机制，为柔性缓冲机构设计提供支撑。

## 1　柔性阵列气囊结构设计

### 1.1　柔性气囊单元设计

本文设计一种带排气孔结构的半球形柔性气囊单元，其结构示意图如图1所示。




(a) 气囊整体结构　　(b) 充/排气孔结构

**图 1　柔性气囊单元结构示意图**

**Fig. 1　Schematic diagram of flexible airbag unit**

该单元的主体为一个外径$R_f$、内径$r_f$、壁厚$t_f$的半球形气囊，该结构设计可通过调控内部气体排放过程，实现碰撞动能的吸收与耗散。气囊底部集成有3个气孔，分别承担预充气、碰撞过程排气及快速排气的功能。当气囊与动态目标发生接触时，排气孔允许内部气体在挤压作用下以受控速率排出，此过程通过气体流动做功耗散碰撞产生的大部分动能，并有效抑制内部气压的急剧升高，实现接触力峰值抑制。当气囊被压缩至最大位移时，为避免储存的弹性势能释放导致目标反弹，快速排气孔立即开启，将剩余气体排出，完成目标物体碰撞动能耗散。

### 1.2　柔性阵列气囊设计

为提高气囊对更大初始碰撞速度适应性能力，基于柔性气囊单元，设计了一种阵列气囊缓冲结构（简称阵列气囊），如图2所示。该柔性阵列气囊基于梯度刚度分布与顺序排气控制策略，实现碰撞动能的多级耗散与接触力峰值调控。

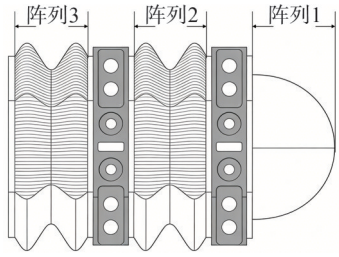



**图 2　柔性阵列气囊结构示意图**

**Fig. 2　Schematic diagram of flexible array airbag structure**

阵列气囊由3个气囊子阵列（阵列1～3）通过刚性中心连接件串联而成，且阵列刚度逐级递增。在碰撞初始阶段，低刚度阵列1首先发生压缩变形，通过内部气体的受控排放完成初始柔顺接触，从而有效截获初始动能并抑制接触力突变。碰撞中期，剩余动能通过刚性中心连接件向后传递，触发阵列2与阵列3依次介入。得益于波纹管状六棱柱气囊结构的高效可压缩性，二级与三级阵列在力传递路径上依次承担主要耗能任务，通过排气进一步耗散剩余动能。刚性中心连接件内部集成的多通路孔道系统为各气囊的充排气过程提供了精确控制，确保气体排放的顺序性与同步性，从而使阵列气囊实现从柔性接触响应到高刚度耗能。

## 2　动力学分析

### 2.1　气囊单元动力学建模

1）气囊有限元模型

由于柔性气囊单元壁厚小，把气囊壁视作为膜，采用Kirchhoff–Love假设对柔性气囊单元进行建模[23–29]。在变形过程中，法线方向保持垂直于中面，厚度始终保持不变，膜的位置状态可以用中面$\Pi_0$来描述。如图3所示，在局部笛卡尔坐标系$O$–$XYZ$中，中面上任意一点$P_r$的位置向量$\boldsymbol{r}$可表示为：

$$\boldsymbol{r}=\boldsymbol{S}_r\boldsymbol{q}_e \tag{1}$$

式中，$\boldsymbol{S}_r$为膜单元的单元形状插值函数矩阵，$\boldsymbol{q}_e$为单元$e$节点坐标的位置向量矩阵。

综合考虑柔性气囊的几何形状、变形特点以及计算精度和效率，采用三角形膜单元进行有限元离散，具体使用三角形面积来描述。

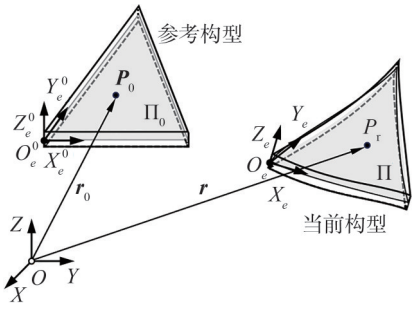



图 3 ANCF 三角膜单元的配置

**Fig. 3 Configuration of ANCF triple corneal unit**

三角形单元面积坐标关系如图 4 所示。

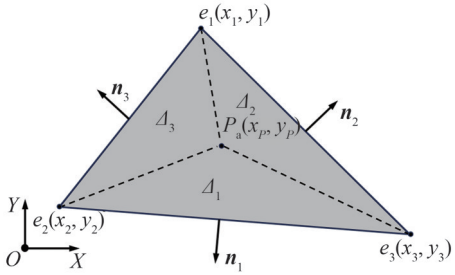


图 4 三角形单元面积坐标关系

**Fig. 4 Coordinate relationship of triangular unit area**

三角形任意一点的位置坐标 $P_a$ 在笛卡尔坐标系 $O$–$XY$ 可以定义为：

$$\begin{cases} x_P = x_1 L_1 + x_2 L_2 + x_3 L_3, \\ y_P = y_1 L_1 + y_2 L_2 + y_3 L_3, \\ L_1 + L_2 + L_3 = 1 \end{cases} \tag{2}$$

式中：$(x_i, y_i)$ 为三角形 3 个顶点的坐标，$i = 1, 2, 3$；$L_i$ 为基于三角形几何面积比例定义的面积坐标，可表示为：

$$L_i = \frac{\Delta_i}{\Delta} = \frac{1}{2\Delta}(c_{i1} x_P + c_{i2} y_P + c_{i3}) \tag{3}$$

式中，$\Delta_i$ 为子三角形的面积，$\Delta$ 为三角形单元的面积，$(c_{i1}, c_{i2})$ 为对边未归一化的内法向量，$c_{i3}$ 由对边截距决定。对于三角形单元上的任意多项式函数 $f(L_1, L_2, L_3)$，其积分可表示为：

$$\int_{\Omega} f(L_1, L_2, L_3)\mathrm{d}\Delta = \Delta \cdot \sum_{i=1}^{3} \omega_i f(L_1^i, L_2^i, L_3^i) \tag{4}$$

式中，$\Omega$ 为积分区域，$\omega_i$ 为积分权重系数，$(L_1^i, L_2^i, L_3^i)$ 为高斯点的面积坐标。

ANCF 三角形膜单元具有 9 个自由度，每个节点包含位置和梯度矢量。单元节点坐标的向量矩阵为：

$$\begin{cases} \boldsymbol{q}_e = \left[\boldsymbol{q}_{e1}^{\mathrm{T}} \quad \boldsymbol{q}_{e2}^{\mathrm{T}} \quad \boldsymbol{q}_{e3}^{\mathrm{T}}\right]^{\mathrm{T}} \in \mathbb{R}^{27\times 1}, \\ \boldsymbol{r}_{ek} = \left[\boldsymbol{r}_k^{\mathrm{T}} \; \boldsymbol{r}_{k,\xi}^{\mathrm{T}} \; \boldsymbol{r}_{k,\eta}^{\mathrm{T}}\right]^{\mathrm{T}}, k = 1, 2, 3, 4 \end{cases} \tag{5}$$

式中，$\boldsymbol{q}_{e1}$~$\boldsymbol{q}_{e3}$ 为三角形单元中节点的矢量坐标，$\boldsymbol{r}_{ek}$ 为全局位置向量，$\boldsymbol{r}_{k,\xi} = \partial \boldsymbol{r}_k / \partial x_P$、$\boldsymbol{r}_{k,\eta} = \partial \boldsymbol{r}_k / \partial y_P$ 为梯度向量。

基于 Specht 的形状插值函数矩阵 $\boldsymbol{S}_{\mathrm{r}}$（$\boldsymbol{S}_{\mathrm{r}} \in \mathbb{R}^{3\times 27}$）可以表示为：

$$\boldsymbol{S}_{\mathrm{r}} = [S_{11}\boldsymbol{I}_3 \quad S_{12}\boldsymbol{I}_3 \quad S_{13}\boldsymbol{I}_3 \quad \cdots \quad S_{32}\boldsymbol{I}_3 \quad S_{33}\boldsymbol{I}_3] \tag{6}$$

式中，$\boldsymbol{I}_3$ 为 3 阶单位矩阵，$S_{ij}(j = 1, 2, 3)$ 的定义详见文献[30]。

膜单元的质量矩阵 $\boldsymbol{M}_e$ 可以定义为：

$$\boldsymbol{M}_e = h\int_A \rho \boldsymbol{S}_{\mathrm{r}}^{\mathrm{T}} \boldsymbol{S}_{\mathrm{r}} \mathrm{d}A \tag{7}$$

式中，$h$ 为膜单元的厚度，$\rho$ 为膜单元的密度，$A$ 为膜单元的中间曲面面积。

给定气囊为各向同性材料，考虑其本构模型，则主应力 $\boldsymbol{\tau}$ 对应的第 2 个 Piola–Kirchhoff 应力张量与主应变 $\boldsymbol{\gamma}$ 对应的格林–拉格朗日应变张量可以表示为：

$$\boldsymbol{\tau} = \boldsymbol{\Gamma}\boldsymbol{\gamma}, \quad \boldsymbol{\tau} = \begin{bmatrix} \sigma_1 \\ \sigma_2 \end{bmatrix}, \quad \boldsymbol{\gamma} = \begin{bmatrix} \gamma_1 \\ \gamma_2 \end{bmatrix} \tag{8}$$

式中，$\boldsymbol{\Gamma}$ 为弹性矩阵，$\sigma_1$ 和 $\sigma_2$ 分别为最大主应力和最小主应力，$\gamma_1$ 和 $\gamma_2$ 分别为最大主应变和最小主应变。$\gamma_1$ 和 $\gamma_2$ 具体形式为：

$$\begin{cases} \gamma_1 = \dfrac{\varepsilon_{11} + \varepsilon_{22}}{2} + \dfrac{1}{2} d^{0.5}, \\ \gamma_2 = \dfrac{\varepsilon_{11} + \varepsilon_{22}}{2} - \dfrac{1}{2} d^{0.5} \end{cases} \tag{9}$$

式中，$d = (\varepsilon_{11} - \varepsilon_{22}) + 4\varepsilon_{12}^2$。膜应变张量 $\boldsymbol{\varepsilon} = [\varepsilon_{11} \quad \varepsilon_{22} \quad 2\varepsilon_{12}]^{\mathrm{T}}$。根据改性皱纹准则[31]，确定膜的应力状态。该方法通过式(10)引入两个参数 $f_1$ 和 $f_2$。

$$\begin{cases} f_1 = \gamma_2 + v\gamma_1, \\ f_2 = \gamma_1 + s_1 v\gamma_2 \end{cases} \tag{10}$$

式中，$v$ 为材料泊松比。根据 $f_1$ 和 $f_2$ 的取值，可以计算弹性矩阵 $\boldsymbol{\Gamma}$，$s_1$ 含义及详细计算步骤参考文献[32]。

因此膜单元弹性力矢量 $\boldsymbol{Q}_{\mathrm{f}}^e$ 可表示为：

$$\boldsymbol{Q}_{\mathrm{f}}^e = -\left(\frac{\partial U_f^e}{\partial \boldsymbol{q}_e}\right)^{\mathrm{T}} = -h\int_A \left[\left(\frac{\partial \gamma_1}{\partial \boldsymbol{q}_e}\right)\left(\frac{\partial \gamma_2}{\partial \boldsymbol{q}_e}\right)\right]\boldsymbol{\Gamma}[\gamma_1 \;\; \gamma_2]^{\mathrm{T}}\mathrm{d}A \tag{11}$$

式中，$U_f^e$ 为弹性势能。

2）气体状态方程

气囊单元系统由气囊、储气瓶、连接储气瓶的圆管道和控制阀组成，如图 5 所示。

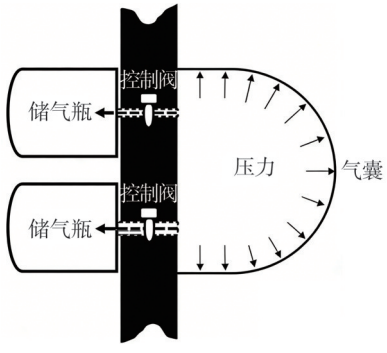



图 5 气囊气体调控系统示意图

**Fig. 5 Schematic diagram of airbag gas control system**

基于控制体积方法，结合理想气体状态方程、质量守恒定律和能量方程，推导气囊气体参数的动态方程[33–34]。

考虑气囊内部气体行为，采用理想气体状态方程描述气体的压强、体积和温度之间的关系，表示如下：

$$PV=mRT \tag{12}$$

式中，$P$为气体的压强，$V$为气体的控制体积，$m$为气体质量，$R$是理想气体常数，$T$为气体温度。

将$m=\rho RT$代入式(12)，得到气囊内气体压强$P$与气体密度$\rho$和温度$T$之间的关系为$P=\rho RT$。

考虑连续性方程，描述气体在充气和排气过程中的流动，气囊气体流量$\dot{m}$可以表示为：

$$\begin{cases}\dot{m}=\dfrac{\mathrm{d}}{\mathrm{d}t}(\rho V),\\ \dot{m}_{\mathrm{in}}-\dot{m}_{\mathrm{out}}=\dot{\rho}V+\rho\dot{V}\end{cases} \tag{13}$$

式中，$\dot{m}_{\mathrm{in}}$和$\dot{m}_{\mathrm{out}}$分别为流入和流出气囊腔体的质量流量，$\dot{\rho}$和$\dot{V}$分别为密度变化率和体积变化率。能量方程用于描述气囊内气体的能量变化，可表示为：

$$\dot{U}=q_{\mathrm{in}}-q_{\mathrm{out}}+YC_V(\dot{m}_{\mathrm{in}}T_{\mathrm{in}}-\dot{m}_{\mathrm{out}}T)-\dot{W} \tag{14}$$

式中，$q_{\mathrm{in}}$和$q_{\mathrm{out}}$为热传递项，$Y$为比热比，$C_V$为定容比热，$T_{\mathrm{in}}$为流入气体的温度，$\dot{U}$为内能变化率，$\dot{W}$为气体做功的变化率。

根据理想气体关系式，将$C_V=R/(Y-1)$、$\dot{W}=P\dot{V}$和$\dot{U}=(V\dot{P}+P\dot{V})/(Y-1)$代入式(14)，得：

$$\frac{1}{Y-1}V\dot{P}=q_{\mathrm{in}}-q_{\mathrm{out}}+\frac{Y}{Y-1}\cdot\frac{P}{\rho T}(\dot{m}_{\mathrm{in}}T_{\mathrm{in}}-\dot{m}_{\mathrm{out}}T)-\frac{Y}{Y-1}P\dot{V} \tag{15}$$

式中，$\dot{P}$为气囊气体压强变化率。

由于接触碰撞的压缩过程时间尺度小，假设气体为绝热模型，忽略气体惯性，则$q_{\mathrm{in}}-q_{\mathrm{out}}=0$，整理式(15)得到$\dot{P}$为：

$$\dot{P}=Y\frac{P}{\rho V}(\dot{m}_{\mathrm{in}}-\dot{m}_{\mathrm{out}})-Y\frac{P}{V}\dot{V} \tag{16}$$

式中，$V$可通过高斯散度定理确定，对气囊表面网格离散得到单元节点，近似表示为：

$$V=\iiint_{\Omega}\mathrm{d}V=\frac{1}{3}\sum_{e}\bar{x}_e\cdot\boldsymbol{n}^eA^e \tag{17}$$

式中，$\bar{x}_e$为膜单元中面面心坐标，$\boldsymbol{n}^e$为单位法向量，$A^e$为单元面积。

气体从高压罐流入气囊的过程中，气体流动受到管道摩擦损失的影响。根据流体力学中的流速计算公式，假设气体流动为层流，流速与管道的长度、直径、气体黏度等因素相关。圆管道层流摩擦损失$B_{\mathrm{pipe}}$通过以下公式计算：

$$B_{\mathrm{pipe}}=\frac{32\mu_{\mathrm{air}}L_{\mathrm{pipe}}v}{\rho gD_{\mathrm{pipe}}^2} \tag{18}$$

式中，$\mu_{\mathrm{air}}$为空气的动力黏度系数，$L_{\mathrm{pipe}}$为管道长度，$v$为管道内平均流速，$g$为重力加速度，$D_{\mathrm{pipe}}$为管道直径。

根据伯努利原理，流入气囊的气体速度计算如下：

$$\frac{p_1}{\rho g}+z_1+\frac{v_1^2}{2g}=\frac{p_2}{\rho g}+z_2+\frac{v_2^2}{2g}+B_{\mathrm{pipe}} \tag{19}$$

式中，$p_1$、$p_2$为管道两端截面的压强，$z_1$、$z_2$为管道两端截面关于同一参考平面的高度，$v_1$、$v_2$为管道两端截面的平均流速。由于管道截面尺寸一致，且位于同一高度，所以$v_1=v_2=v$，$z_1=z_2$，可以得到通过管道流入气囊的平均流速$v$为：

$$v=\frac{(p_1-p_2)D_{\mathrm{pipe}}^2}{32\mu_{\mathrm{air}}L_{\mathrm{pipe}}} \tag{20}$$

根据上述气体流动速度的计算公式，结合气体流速$v$、气体密度$\rho$和管道横截面积$A=\pi D_{\mathrm{pipe}}^2/4$，可以计算出气体质量流量$\dot{m}$：

$$\dot{m}=\frac{\pi\rho(p_1-p_2)D_{\mathrm{pipe}}^4}{128\mu_{\mathrm{air}}L_{\mathrm{pipe}}} \tag{21}$$

在离散的三角形膜单元模型中，假设每个单元受到均匀气压$P$，联立式(16)和(21)可以求得$P$，则该膜单元上气压引起的等效力$\boldsymbol{Q}_P^e$可表示为：

$$\boldsymbol{Q}_P^e=P\cdot\boldsymbol{n}^e\cdot A^e \tag{22}$$

3)碰撞接触力模型

考虑接触碰撞时柔性气囊和刚体的接触为正接触，假设其为无摩擦接触问题以简化计算。本文采用GGEOM(General GEOMetry)接触算法[35]，在改进的柔顺接触力模型中，接触法向力被分解为弹簧力$f_{\mathrm{k}}$和阻尼力$f_{\mathrm{d}}$，定义如下：

$$\begin{cases}f_{\mathrm{k}}=k_{\mathrm{s}}\delta^n,\\ f_{\mathrm{d}}=\lambda\delta^n\dot{\delta}\end{cases} \tag{23}$$

式中：$k_{\mathrm{s}}$和$n$分别为接触刚度参数和接触非线性幂指数，由实验测得；$\delta$为穿透深度；$\lambda$为阻尼系数；$\dot{\delta}$为穿透速率。推导出节点之间的接触法向力$f_{\mathrm{c}}^l$为：

$$f_{\mathrm{c}}^l=f_{\mathrm{k}}^l+f_{\mathrm{d}}^l \tag{24}$$

式中，$l$为节点编号。

对所有发生接触的节点接触力进行有限元组装，则广义接触力$\boldsymbol{Q}_{\mathrm{c}}$可表示为：

$$\boldsymbol{Q}_{\mathrm{c}}=\sum_{l=1}^{u}\boldsymbol{L}^lf_{\mathrm{c}}^l \tag{25}$$

式中，$\boldsymbol{L}^l$为将局部节点自由度映射至全局系统自由度的布尔矩阵，$u$为离散节点数量。

图6为GGEOM算法的流程图。

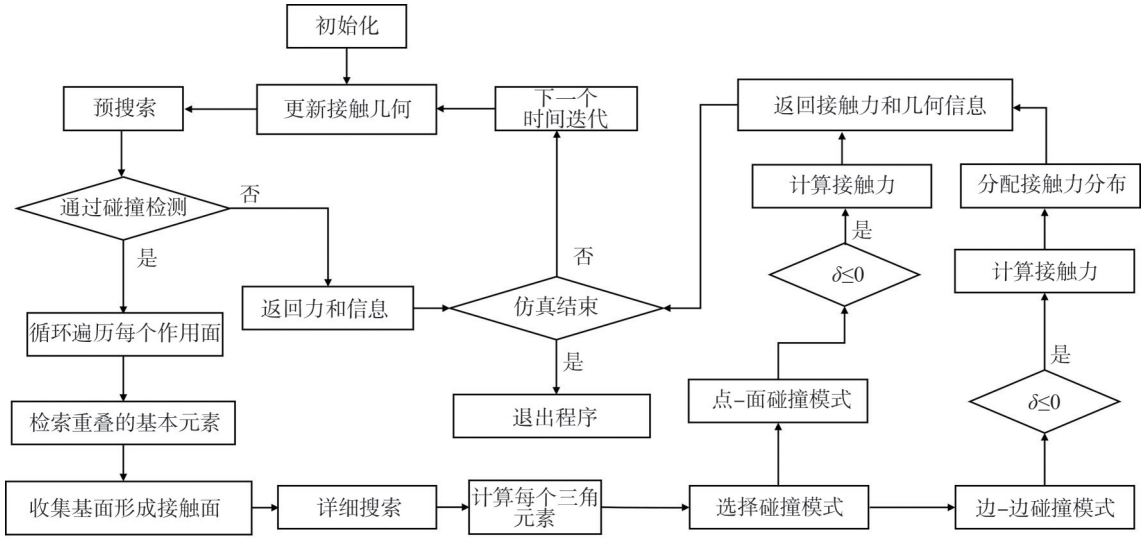



**图 6 GGEOM算法流程图**

**Fig. 6 GGEOM algorithm flowchart**

### 2.2 阵列气囊动力学模型

对阵列气囊进行动力学建模，模型示意图见图7。其中，阵列1柔性单元采用有限元方法建模，阵列2和阵列3采用非线性弹簧阻尼模型进行建模。模型适用于阵列气囊在中低速碰撞条件下的动力学分析，假设气体过程为绝热过程，忽略气体惯性与摩擦接触效应。

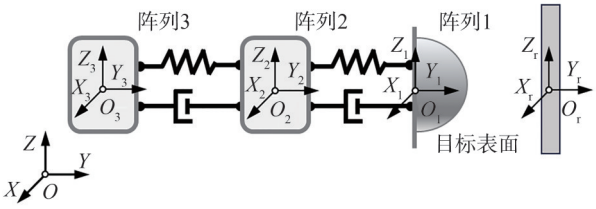



**图 7 阵列气囊模型示意图**

**Fig. 7 Schematic diagram of array airbag model**

在接触碰撞过程中，碰撞目标的运动采用笛卡尔坐标系描述，其广义坐标矩阵可以表示为：

$$\boldsymbol{q}_{\mathrm{r}}=\left[\boldsymbol{r}_{\mathrm{c}}^{\mathrm{T}}\quad\boldsymbol{q}_{\mathrm{rot}}^{\mathrm{T}}\right]^{\mathrm{T}} \tag{26}$$

式中，$\boldsymbol{r}_{\mathrm{c}}$为刚体质心的全局位置向量，$\boldsymbol{q}_{\mathrm{rot}}$为用来描述刚体的旋转的四元数坐标。

定义连接矩阵$\boldsymbol{B}_e$，阵列1气囊单元的广义坐标矩阵$\boldsymbol{q}_e$可以由节点广义坐标向量$\boldsymbol{q}_l$给出，即$\boldsymbol{q}_e=\boldsymbol{B}_e\boldsymbol{q}_l$。

阵列1的广义坐标矩阵$\boldsymbol{q}_{\mathrm{f}}$可以表示为：

$$\boldsymbol{q}_{\mathrm{f}}=\left[\boldsymbol{q}_1^{\mathrm{T}}\quad\boldsymbol{q}_2^{\mathrm{T}}\quad\cdots\quad\boldsymbol{q}_u^{\mathrm{T}}\right]^{\mathrm{T}} \tag{27}$$

联立式(7)，气囊质量矩阵$\boldsymbol{M}_{\mathrm{f}}$可以表示为：

$$\boldsymbol{M}_{\mathrm{f}}=\sum_e\boldsymbol{B}_e^{\mathrm{T}}\boldsymbol{M}_e\boldsymbol{B}_e \tag{28}$$

阵列2和阵列3等效为集中质量矩阵$\boldsymbol{M}_2$和$\boldsymbol{M}_3$的刚体运动，采用笛卡尔坐标系描述，则其广义坐标矩阵$\boldsymbol{q}_{\mathrm{r23}}$可以表示为：

$$\boldsymbol{q}_{\mathrm{r23}}=\left[\boldsymbol{r}_{\mathrm{c23}}^{\mathrm{T}}\quad\boldsymbol{q}_{\mathrm{rot23}}^{\mathrm{T}}\right]^{\mathrm{T}} \tag{29}$$

式中，$\boldsymbol{r}_{\mathrm{c23}}$为集中质量矩阵$\boldsymbol{M}_2$和$\boldsymbol{M}_3$的全局位置向量，$\boldsymbol{q}_{\mathrm{rot23}}$为用来描述旋转的四元数坐标。

系统的广义坐标矩阵$\boldsymbol{q}$为：

$$\boldsymbol{q}=\left[\boldsymbol{q}_{\mathrm{r}}^{\mathrm{T}}\quad\boldsymbol{q}_{23}^{\mathrm{T}}\quad\boldsymbol{q}_{\mathrm{f}}^{\mathrm{T}}\right]^{\mathrm{T}} \tag{30}$$

系统的广义质量矩阵$\boldsymbol{M}$为：

$$\boldsymbol{M}=\mathrm{diag}(\boldsymbol{M}_{\mathrm{r}},\boldsymbol{M}_{23},\boldsymbol{M}_{\mathrm{f}}) \tag{31}$$

式中，$\boldsymbol{M}_{\mathrm{r}}$和$\boldsymbol{M}_{23}$分别为碰撞目标和阵列2、3的质量矩阵。

系统的广义力$\boldsymbol{Q}$可写成：

$$\boldsymbol{Q}=\boldsymbol{Q}_{\mathrm{f}}+\boldsymbol{Q}_{\mathrm{c}}+\boldsymbol{Q}_P+\boldsymbol{f}_{\mathrm{KD}} \tag{32}$$

式中：$\boldsymbol{Q}_{\mathrm{f}}=\sum_e\boldsymbol{B}_e^{\mathrm{T}}\boldsymbol{Q}_{\mathrm{f}}^e$；$\boldsymbol{Q}_P=\sum_e\boldsymbol{B}_e^{\mathrm{T}}\boldsymbol{Q}_P^e$，$\boldsymbol{Q}_{\mathrm{f}}^e$、$\boldsymbol{Q}_P^e$、$\boldsymbol{Q}_{\mathrm{c}}$分别由式(11)、(22)、(25)给出，$\boldsymbol{f}_{\mathrm{KD}}$为阵列2和3的等效刚度阻尼力。为考虑内部和外部的耗散影响，柔性单元结构采用了Rayleigh阻尼模型。系统的阻尼力可表示为：

$$\boldsymbol{f}_{\mathrm{D}}=\boldsymbol{C}\dot{\boldsymbol{q}} \tag{33}$$

式中，$\boldsymbol{C}$为阻尼矩阵，在大变形分析中可简化为$\boldsymbol{C}=\alpha\boldsymbol{M}$，其中，$\alpha$为质量比例阻尼系数。

系统引入约束方程$\boldsymbol{\Phi}=0$，基于第一类拉格朗日方程导出多体系统的动力学方程如下：

$$\begin{cases}\boldsymbol{M}\ddot{\boldsymbol{q}}+\boldsymbol{f}_{\mathrm{D}}-\boldsymbol{Q}+\boldsymbol{\Phi}_{\boldsymbol{q}}^{\mathrm{T}}\lambda=0,\\ \boldsymbol{\Phi}=0\end{cases} \tag{34}$$

式中，$\ddot{\boldsymbol{q}}$为节点广义加速度矩阵，$\boldsymbol{\Phi}_{\boldsymbol{q}}=\partial\boldsymbol{\Phi}/\partial\boldsymbol{q}$为雅可比矩阵，$\lambda$为拉格朗日乘子。

## 3 阵列气囊碰撞响应特性分析

为分析所提出的阵列气囊结构碰撞接触能量传递和接触力演变规律，基于第2.2节的模型开展了仿

真和实验研究。阵列气囊与碰撞目标的主要参数如表1所示。考虑较低初始动能（场景1）和高初始动能（场景2）下的接触碰撞场景，设计两组实验工况，实验工况参数见表2。气浮微重力实验平台如图8所示。

**表1　阵列气囊与碰撞目标的主要参数**

**Tab. 1　Main parameters of array airbags and targets**

| 阵列 | 参数 | 取值 |
|---|---|---|
| 阵列1 | 基座质量/kg | 6 |
| | 基座几何尺寸/(mm×mm×mm) | 365×140×140（长×宽×高） |
| | 气囊质量/g | 50 |
| | 气囊几何尺寸/mm | 35/1.5（半径/厚度） |
| | 气囊初始压力/MPa | 0.101 |
| 阵列2 | 气囊质量/g | 50 |
| | 气囊几何尺寸/mm | 20（长） |
| 阵列3 | 气囊质量/g | 50 |
| | 气囊几何尺寸/mm | 20（长） |
| 碰撞目标 | 质量/kg | 300 |
| | 几何尺寸/(mm×mm×mm) | 1 000×1 000×1 000 |

**表2　实验工况参数**

**Tab. 2　Experimental condition parameters**

| 场景 | 工况 | 初始动能/J | 初始相对接触速度/($m\cdot s^{-1}$) | 阵列1、2、3预充压力/MPa |
|---|---|---|---|---|
| 场景1 | 1 | 0.5 | 0.36 | 0、0.01、0.02 |
| | 2 | 0.5 | 0.36 | 0、0.01、0.04 |
| | 3 | 0.5 | 0.36 | 0、0.03、0.04 |
| 场景2 | 4 | 1.2 | 0.63 | 0、0.01、0.02 |
| | 5 | 1.2 | 0.63 | 0、0.01、0.04 |
| | 6 | 1.2 | 0.63 | 0、0.03、0.04 |



**图8　气浮微重力实验平台**

**Fig. 8　Air flotation microgravity experimental platform**

为确保研究的合理性与工程适用性，表1和表2中的主要参数选取考虑了微重力气浮试验平台（图8）能力约束以及未来在轨捕获任务的快响应需求等因素。其中，气囊阵列的几何尺寸、质量特性、运动速度等参数依据模拟器的安装接口、包络空间、重力卸载和模拟器的最大运动速度与动能上限确定，以保证集成后不干扰试验系统的动力学行为。

1）场景1

在初始动能为0.5 J时，不同预充压力下阵列气囊碰撞能量耗散响应特性和接触力响应特性分别如图9、10所示。由图9可以看出，仿真结果的能量耗散时间略短于实验结果，这是由于模型对气体流动和材料行为进行了简化处理，未考虑气体流动损失及材料黏弹性效应，使仿真中的能量耗散过程略快于实验。

根据碰撞过程中动能演化与阵列气囊工作机制，从能量耗散曲线上看，碰撞过程可划分为3个阶段：a）初始接触阶段（0～50 ms），阵列1主导排气，实现柔顺接触并初步吸收动能；b）主要耗散阶段（50～200 ms），阵列2与阵列3依次介入，通过受控排气快速耗散剩余动能；c）稳定阶段（200 ms后），动能趋近于0，系统恢复平稳。由图10可知，接触力峰值随着预充压力增大而增大，接触力峰值由单位接触面积归一化表示，单位为$N/cm^2$。通过调节不同的预充压力组合，可有效降低峰值力，最小峰值力为0.9 $N/cm^2$。

2）场景2

在初始动能为1.2 J时，不同预充压力下阵列气囊的接触力响应特性如图11所示。在较高初始动能条件下，接触力峰值随着预充压力增大而增大，并且通过调节不同预充压力组合，有效降低峰值力，最小峰值力为1.1 $N/cm^2$。

场景1、2的实验结果表明，当初始动能分别为0.5、1.2 J时，通过不同的预充介质气压组合可以有效地将接触力峰值分别降低至0.9 $N/cm^2$和1.1 $N/cm^2$，预充介质气压越大，接触力峰值相应增大。其本质原因是，填充介质预充气压的提升会使系统等效刚度增加，导致结构表现出更强的刚性特征，进而使得碰撞过程中的接触力峰值显著提高。

对比场景1、2的仿真与实验结果，模型预测误差小于10%，仿真与实验曲线的整体变化趋势基本一致，但结果存在一定差异。仿真曲线在主要耗散阶段通常略高于实验，且在高压工况下更为明显。这种差异主要源于气体流动采用理想层流模型，气囊材料参数存在实验测量误差，以及接触刚度与阻尼参数辨识存在不确定性。特别是在高压条件下，气囊材料的非线性变形与接触面的相互作用更为显著，导致仿真与实验的偏差增大。

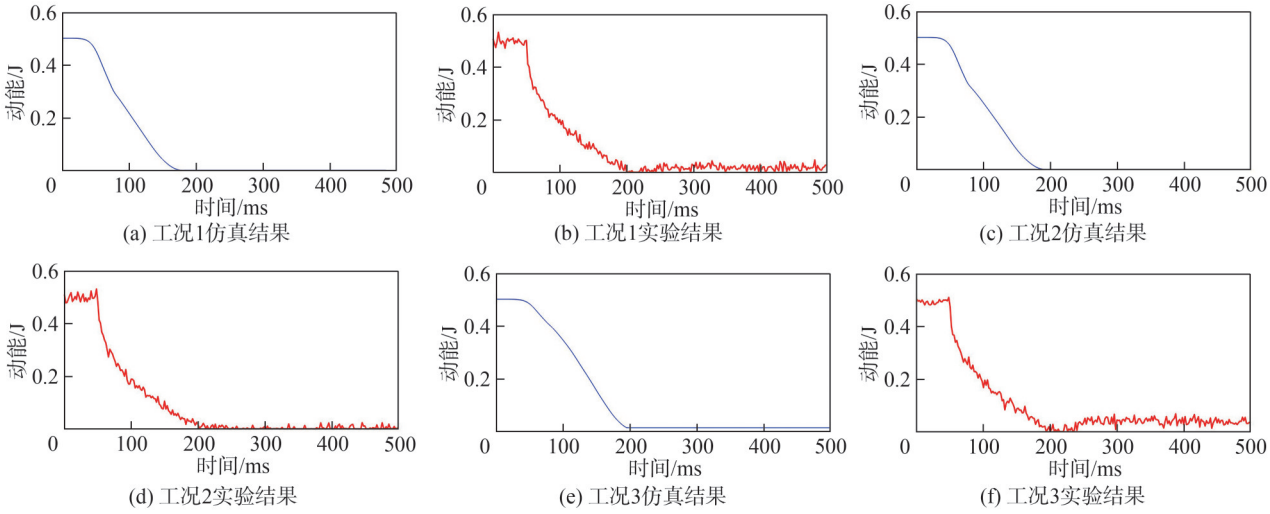



图 9 不同预充压力下阵列气囊碰撞能量耗散响应特性(场景 1)

**Fig. 9 Collision energy dissipation response characteristics of array airbags under different precharge pressures (Scenario 1)**

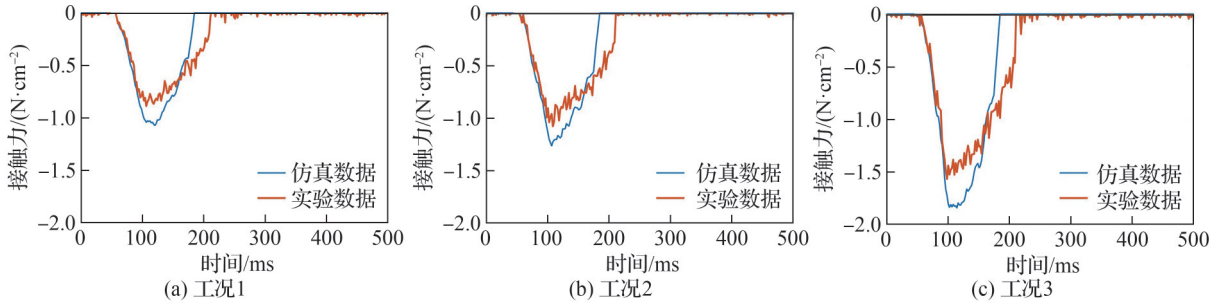



图 10 不同预充压力下阵列气囊接触力响应特性(场景 1)

**Fig. 10 Response characteristics of contact force of array airbag under different precharge pressures (Scenario 1)**

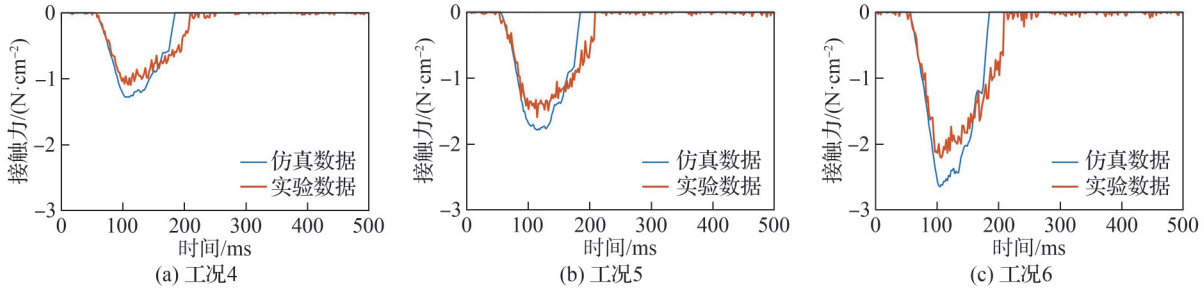



图 11 不同预充压力下阵列气囊接触力响应特性(场景 2)

**Fig. 11 Response characteristics of contact force of array airbag under different precharge pressures (Scenario 2)**

## 4 结 论

本文提出基于多气囊协同的阵列气囊缓冲结构,考虑气囊结构大变形、内部气体状态变化、非线性接触,建立了阵列气囊结构的动力学模型,通过数值仿真与实验分析,得出以下主要结论:

1) 提出了阵列式气囊结构,通过多气囊协同变形与气体压缩优化系统接触力响应特性,实现了接触碰撞过程中的能量快速耗散和接触力抑制。

2) 建立了阵列气囊结构的系统动力学模型,仿真与实验结果表明,阵列气囊结构在初始动能为 1.2 J 以内碰撞条件下,通过调节不同预充压力组合,能有效降低接触力峰值至 1.1 N/cm$^2$,能量耗散率达 95% 以上,模型预测误差小于 10%。

未来将考虑空间温度、真空、微重力等因素,研究多阵列气囊智能协同机制、动力学响应特性与控制方法,为在轨接触式捕获缓冲装置设计与性能提升提供支撑。

**参考文献:**

[1] Ma Boyu, Jiang Zainan, Liu Yang, et al. Advances in space robots for on-orbit servicing: A comprehensive review[J]. Advanced Intelligent Systems, 2023, 5(8): 2200397.

[2] Papadopoulos E, Aghili F, Ma Ou, et al. Robotic manipulation and capture in space: A survey[J]. Frontiers in Robot-

ics and AI,2021,8:686723.

[3] Flores-Abad A, Zhang Lin, Wei Zheng, et al. Optimal capture of a tumbling object in orbit using a space manipulator[J]. Journal of Intelligent & Robotic Systems, 2017, 86(2): 199–211.

[4] Liu Xiaofeng, Cai Guoping, Wang Mingming, et al. Contact control for grasping a non-cooperative satellite by a space robot[J].Multibody System Dynamics,2020,50(2):119–141.

[5] Sun Yongjun, Wang Qian, Liu Yiwei, et al. A survey of non-cooperative target capturing methods[J]. Journal of National University of Defense Technology,2020,42(3):74–90. [孙永军,王钤,刘伊威,等 . 空间非合作目标捕获方法综述[J]. 国防科技大学学报,2020,42(3):74–90.]

[6] Phipps C R.A laser-optical system to re-enter or lower low Earth orbit space debris[J].Acta Astronautica,2014,93: 418–429.

[7] Bombardelli C, Pelaez J. Ion beam shepherd for contactless space debris removal[J]. Journal of Guidance, Control, and Dynamics,2011,34(3):916–920.

[8] Shan Minghe, Guo Jian, Gill E. Review and comparison of active space debris capturing and removal methods[J]. Progress in Aerospace Sciences,2016,80:18–32.

[9] Pan Zhengwei. The design and dynamics analysis of capturing mechanism for the uncooperative target satelites[D]. Nanjing: Nanjing University of Aeronautics and Astronautics,2017.[潘正伟 . 空间非合作目标捕获机构设计及动力学分析[D]. 南京:南京航空航天大学,2017.]

[10] Sun Chong, Yuan Jianping, Wan Wenya, et al. Outside envelop grasping method and approaching trajectory optimization for tumbling malfunctional satellite capture[J]. Acta Aeronautica et Astronautica Sinica, 2018, 39(11): 322203. [孙冲,袁建平,万文娅,等 . 自由翻滚故障卫星外包络抓捕及抓捕路径优化[J]. 航空学报,2018,39(11):322203.]

[11] Yin Hang, Zeng Guoqiang, Gao Yongming, et al. On-orbit capture TechnoIogy for non-cooperative target based on FIexibIe joint[J]. Journal of Academy of Equipment, 2013, 24(6): 69–72.[尹航,曾国强,高永明,等 . 基于柔性关节的非合作目标在轨捕获技术及仿真[J]. 装备学院学报, 2013,24(6):69–72.]

[12] Zhang Yin, Zhang Wang, Gao Pan, et al. Finger-palm synergistic soft gripper for dynamic capture *via* energy harvesting and dissipation[J]. Nature Communications, 2022,13: 7700.

[13] Borase R P, Maghade D K, Sondkar S Y, et al. A review of PID control, tuning methods and applications[J]. International Journal of Dynamics and Control,2021,9(2):818–827.

[14] Nenchev D N, Yoshida K. Impact analysis and post-impact motion control issues of a free-floating Space robot subject to a force impulse[J]. IEEE Transactions on Robotics and Automation,1999,15(3):548–557.

[15] Dong Qiuhuang, Chen Li. Impact effect analysis of dual-arm space robot capturing a non-cooperative target and force/position robust stabilization control for closed-chain hybrid system[J].Journal of Mechanical Engineering,2015, 51(9):37–44.[董楸煌,陈力 . 双臂空间机器人捕获非合作目标冲击效应分析及闭链混合系统力/位形鲁棒镇定控制[J]. 机械工程学报,2015,51(9):37–44.]

[16] Dong Fuxiang, Hong Jiazhen. Review of impact problem for dynamics of multibody system[J]. Advances in Mechanics, 2009,39(3):352–359.[董富祥,洪嘉振 . 多体系统动力学碰撞问题研究综述[J]. 力学进展,2009,39(3):352–359.]

[17] Hertz H. Über die Berührung fester elastischer Körper[J]. Journal für die reine und angewandte Mathematik, 1881, 92:156–171.

[18] Hunt K H, Crossley F R E. Coefficient of restitution interpreted as damping in vibroimpact[J]. Journal of Applied Mechanics,1975,42(2):440–445.

[19] Lankarani H M, Nikravesh P E. A Contact force model with hysteresis damping for impact analysis of multibody systems[J]. Journal of Mechanical Design, 1990, 112(3):369 –376.

[20] Gonthier Y, McPhee J, Lange C, et al. A regularized contact model with asymmetric damping and dwell-time dependent friction[J]. Multibody System Dynamics, 2004, 11(3): 209–233.

[21] Flores P, Machado M, Silva M T, et al. On the continuous contact force models for soft materials in multibody dynamics [J].Multibody System Dynamics,2011,25(3):357–375.

[22] Gharib M, Hurmuzlu Y. A new contact force model for low coefficient of restitution impact[J]. Journal of Applied Mechanics,2012,79(6):064506.

[23] Campanelli M, Berzeri M, Shabana A A. Performance of the incremental and non-incremental finite element formulations in flexible multibody problems[J]. Journal of Mechanical Design,2000,122(4):498-507.

[24] Shabana A A. An absolute nodal coordinate formulation for the large rotation and deformation analysis of flexible bodies: MBS96-1-UIC[R]. Chicago: Department of Mechanical Engineering, University of Illinois at Chicago,1996.

[25] Mikkola A M, Shabana A A. A non-incremental finite element procedure for the analysis of large deformation of plates and shells in mechanical system applications[J]. Multibody System Dynamics,2003,9(3):283–309.

[26] Dmitrochenko O N, Pogorelov D Y. Generalization of plate finite elements for absolute nodal coordinate formulation [J].Multibody System Dynamics,2003,10(1):17–43.

[27] Sanborn G G,Choi J,Choi J H.Curve-induced distortion of polynomial space curves,flat-mapped extension modeling, and their impact on ANCF thin-plate finite elements[J]. Multibody System Dynamics,2011,26(2):191–211.

[28] Liu Xinxiang, Jenkins C H, Schur W W. Large deflection analysis of pneumatic envelopes using a penalty parameter modified material model[J]. Finite Elements in Analysis and Design,2001,37(3):233–251.

[29] Dmitrochenko O, Mikkola A. Two simple triangular plate elements based on the absolute nodal coordinate formulation[J].Journal of Computational and Nonlinear Dynamics, 2008,3(4):041012.

[30] Specht B. Modified shape functions for the three-node plate bending element passing the patch test[J]. International Journal for Numerical Methods in Engineering, 1988,26(3):705–715.

[31] Miyazaki Y. Wrinkle/slack model and finite element dynamics of membrane[J]. International Journal for Numerical Methods in Engineering,2006,66(7):1179–1209.

[32] Yuan Tingting, Liu Zhuyong, Zhou Yuhang, et al. Dynamic modeling for foldable origami space membrane structure with contact-impact during deployment[J]. Multibody System Dynamics,2020,50(1):1–24.

[33] Xue Suduo, Yan Fei, Sun Guojun. Deflation and collapse of air-supported membrane structures[J]. Thin-Walled Structures,2021,169:108338.

[34] Lampani L, Gaudenzi P. Numerical simulation of the behavior of inflatable structures for space[J]. Acta Astronautica,2010,67(3/4):362–368.

[35] Choi J, Rhim S, Choi J H. A general purpose contact algorithm using a compliance contact force model for rigid and flexible bodies of complex geometry[J]. International Journal of Non-Linear Mechanics,2013,53:13–23.

## Characteristics Analysis of Collision Energy Dissipation and Contact Force Suppression of Arrayed Airbags

*ZHONG You*[1,2], *YANG Siyun*[1,2], *XUE Miao*[1,2], *TANG Lei*[1,2], *PU Wei*[1,2,3*], *ZHANG Yin*[1,2*]

(1.School of Astronautics and Aeronautics, Sichuan University, Chengdu 610207, China;
2.Key Laboratory of Advanced Spatial Mechanism and Intelligent Spacecraft, Ministry of Education, Chengdu 610207, China;
3.School of Mechanical Engineering, Sichuan University, Chengdu 610065, China)

**Abstract**:

**Objective** Collision disturbances arising during contact operations pose a critical challenge in on-orbit servicing, spacecraft maintenance, and space debris removal missions. During the capture of noncooperative targets, unavoidable physical contact between the servicing spacecraft and the target can generate substantial impact forces, potentially resulting in structural damage or mission failure. Conventional rigid damping mechanisms, including spring-based and electromagnetic damping systems, are widely employed because of their rapid response and relatively high energy dissipation efficiency. However, their inherent rigidity limits their adaptability to different collision velocities and dynamic impact conditions, restricting their applicability in complex space operations. Flexible buffering structures attract increasing attention because their compliant properties enable adaptive deformation and energy absorption during collisions. Among various flexible buffering mechanisms, pneumatic airbag structures provide distinct advantages owing to the compressibility of their internal gas and the adjustable mechanical properties achieved through internal pressure regulation. However, the collision response mechanisms and energy dissipation characteristics of multi-airbag systems remain insufficiently understood, particularly when multiple airbags during dynamic contact processes. In this study, we aimed to propose a flexible array airbag buffering structure that suppresses contact forces and dissipates collision energy during capture operations. A dynamic model of the airbag unit and multilevel array structure is established to examine the effects of key parameters on collision response behavior. In addition, we seeked to clarify the mechanisms governing energy dissipation and contact force transmission in a collaborative multi-airbag system.

**Methods** A hemispherical flexible airbag unit equipped with controlled exhaust ports was designed to provide adaptive energy dissipation during collisions. The airbag structure enabled the controlled release of compressed gas during impact, which facilitated effective collision energy dissipation while limiting increases in internal pressure. A hierarchical airbag array structure was further proposed to improve buffering performance and extend the applicable range of collision energies. The array comprised three coordinated subarrays with distinct structural characteristics. The first array interacted directly with the collision interface and provided initial compliant buffering. The second and third arrays incorporated corrugated prism-shaped airbags that served as secondary and tertiary buffering units, respectively. These multilevel airbags were connected through a rigid central support structure, which maintained stable positioning and provided channels for gas supply and exhaust. A dynamic model of the airbag system was developed by considering structural deformation, changes in the internal gas state, and nonlinear contact interactions. The flexible airbag membrane was modeled using the absolute nodal coordinate formulation, with triangular membrane elements based on the Kirchhoff-Love assumption. This approach enabled accurate representation of the large-deformation behavior of thin-walled membranes. The internal gas behav-

ior was described using the ideal gas state equation in combination with mass conservation and energy balance equations. The compression process during collision was assumed to be adiabatic because of the short impact duration. Gas inflow and outflow through the connecting pipelines were modeled using fluid mechanics relationships that accounted for pressure-driven flow through circular channels. The contact interaction between the airbag and the rigid target was represented using a nonlinear compliant contact model implemented through the general geometry contact algorithm. The contact force comprised elastic and damping components that depended on penetration depth and velocity. The dynamic equations of the coupled system were formulated using Lagrange multipliers to incorporate system constraints. Numerical simulations were conducted to investigate collision responses under different combinations of initial kinetic energy and preinflation pressure. Collision experiments were performed using an air flotation microgravity simulation platform to validate the numerical model. Two representative collision scenarios were examined, with initial kinetic energies of 0.5 J and 1.2 J. Different preinflation pressure combinations were tested to evaluate their effects on energy dissipation efficiency and peak contact force.

**Results and Discussions** Simulation and experimental results demonstrated consistent trends in collision response behavior under different pressure configurations. The kinetic energy dissipation process was characterized by three stages: the initial contact, the main energy dissipation, and the stabilization stages. During the initial contact stage, the first airbag array underwent compliant deformation and reduced the initial impact force. As the collision progressed, the secondary and tertiary airbag arrays became engaged, which facilitated multilevel buffering and the gradual dissipation of the remaining kinetic energy. Under the 0.5 J collision condition, the system exhibited stable energy dissipation characteristics across different preinflation pressure combinations. The kinetic energy remained nearly constant during the first 50 ms, which corresponded to the initial deformation stage. A rapid reduction in energy occurred between 50 and 60 ms as multiple airbags underwent simultaneous compression. Then, the remaining energy decreased gradually and approached zero at approximately 200 ms. The corresponding contact force responses demonstrated that the peak impact force increased with increasing preinflation pressure. Adjustments to the pressure combinations of the airbag arrays effectively suppressed the peak contact force. Under optimized pressure configurations, the minimum peak contact force reached approximately 0.9 N/cm$^2$. Similar trends were observed under the higher-energy collision scenario, with an initial kinetic energy of 1.2 J. The multilevel buffering mechanism remained effective, and the minimum peak contact force was approximately 1.1 N/cm$^2$. These findings indicated that the airbag array structure maintained stable collision mitigation performance across a range of impact conditions. Comparisons between the simulation and experimental results demonstrated good agreement in the overall trends, with prediction errors below 10%. Minor discrepancies were observed in the duration of energy dissipation, as the simulation curves exhibited slightly faster energy decay than the experimental measurements. This difference was primarily attributed to simplified modeling assumptions, including idealized gas flow behavior, the omission of material viscoelastic effects, and simplified contact interaction models. Despite these discrepancies, the numerical model effectively captured the dominant characteristics of collision energy transfer and contact force evolution, demonstrating its capability to predict the dynamic response of the airbag array system.

**Conclusions** A flexible array airbag buffering structure was proposed to suppress collision disturbances during spacecraft capture operations. A coupled dynamic model accounting for large membrane deformation, gas state evolution, and nonlinear contact interactions was developed to analyze collision response behavior. Numerical simulations and experimental validation demonstrated that the proposed array airbag structure effectively dissipated collision energy through multilevel cooperative deformation and gas compression mechanisms. The peak contact force can be significantly reduced while maintaining high energy dissipation efficiency by adjusting preinflation pressure combinations. Under collision conditions with initial kinetic energy of up to 1.2 J, the array airbag structure achieved energy dissipation rates exceeding 95%, and peak contact forces were reduced to approximately 1.1 N/cm$^2$. The simulation model demonstrated good agreement with experimental observations, with prediction errors below 10%. These findings indicate that multi-airbag cooperative buffering provides an effective approach to mitigating collision disturbances during contact capture processes. The proposed modeling framework also provides a theoretical basis for designing and optimizing flexible buffering mechanisms in spacecraft capture systems. Future work will further examine the influence of environmental conditions and structural parameters on the performance of airbag arrays, including the effects of vacuum environments, material properties, and complex collision scenarios.

**Key words**: arrayed airbags; dynamic modeling; contact force; energy dissipation; on-orbit servicing

（编辑　陈　雪）

引用格式: Zhong You,Yang Siyun,Xue Miao,et al.Characteristics analysis of collision energy dissipation and contact force suppression of arrayed airbags[J].Advanced Engineering Sciences,2026,58(6):340–349.[钟友,杨思昀,薛淼,等.阵列气囊碰撞能量耗散与接触力抑制特性分析[J].工程科学与技术,2026,58(6):340–349.]